ACS OMEGA

http://pubs.acs.org/journal/acsodf

Article

Corn Silk Polysaccharides with Different Carboxyl Contents Reduce the Oxidative Damage of Renal Epithelial Cells by Inhibiting Endocytosis of Nano-calcium Oxalate Crystals

Yi-Han Zhang, Chun-Yao Li, Guo-Jun Zou, Jun-Yi Xian, Quan Zhang, Bang-Xian Yu, Ling-Hong Huang, Hong-Xing Liu,* and Xin-Yuan Sun*

Cite This: *ACS Omega* 2023, 8, 25839−25849

Read Online

ACCESS | Metrics & More | Article Recommendations

ABSTRACT: Objective: Renal epithelial cell injury and cell−crystal interaction are closely related to kidney stone formation. Methods: This study aims to explore the inhibition of endocytosis of nano-sized calcium oxalate monohydrate (nano-COM) crystals and the cell protection of corn silk polysaccharides (CCSPs) with different carboxyl contents (3.92, 7.75, 12.90, and 16.38%). The nano-COM crystals protected or unprotected by CCSPs were co-cultured with human renal proximal tubular epithelial cells (HK-2), and then the changes in the endocytosis of nano-COM and cell biochemical indicators were detected. Results: CCSPs could inhibit the endocytosis of nano-COM by HK-2 cells and reduce the accumulation of nano-COM in the cells. Under the protection of CCSPs, cell morphology is restored, intracellular superoxide dismutase levels are increased, lipid peroxidation product malondialdehyde release is decreased, and mitochondrial membrane potential and lysosomal integrity are increased. The release of Ca^{2+} ions in the cell, the level of cell autophagy, and the rate of cell apoptosis and necrosis are also reduced. CCSPs with higher carboxyl content have better cell protection abilities. Conclusion: CCSPs could inhibit the endocytosis of nano-COM crystals and reduce cell oxidative damage. CCSP3, with the highest carboxyl content, shows the best biological activity.

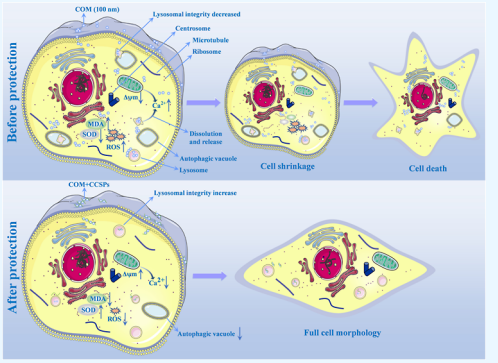

1. INTRODUCTION

Kidney stones are a common and frequently occurring disease worldwide, and their incidence is increasing year by year.[1,2] About 95% of kidney stones are crystalline, with only 5% of the stone contributed by organic components (matrix or proteins).[3] The crystalline component of kidney stones in most of China was calcium oxalate (CaOx; 65.9%), carbapatite (15.6%), urate (12.4%), struvite (2.7%), and brushite (1.7%).[4] Calcium oxalate (CaOx) is the main pathogenic crystalline component. Among them, the thermodynamically stable monoclinic system calcium oxalate monohydrate (COM) has a higher incidence rate of kidney stones and a greater risk of stone formation than the metastable tetragonal system calcium oxalate dihydrate (COD).[5,6]

CaOx crystals that adhered to the cell surface could be endocytosed into cells under the action of microvilli within 30 min.[7] Endocytosis is an energy-dependent process in which vesicles produced through the plasma membrane take up substances from the extracellular environment.[8] At present, the role of cells' endocytosis of external crystals in the process of stone formation is still unclear. Reports have shown that adhered crystals could be transferred to lysosomes through endocytosis and then dissolved within 48 h under the action of acid hydrolase, thereby reducing the toxicity of crystals to renal tubular cells.[9] Studies have also shown that the cytotoxicity of CaOx is positively correlated with the number of endocytosed crystals in a higher concentration range.[10] The endocytosed crystals could directly interact with the lysosome in the cell, causing the lysosome to rupture, releasing a large amount of Ca^{2+} and Ox^{2-}, and then causing cell damage. The endocytosis of a small amount of external particles could reduce the adhesion of the cell surface; however, when an excessive amount of crystals is endocytosed to exceed the digestive capacity of the cell itself, it could cause cell damage or even death.[10,11]

At present, the clinical drugs used to treat or prevent kidney stones mainly include thiazide diuretics, citrate supplements, and cysteine-conjugated drugs (such as D-penicillamine and tiopronin); however, the current incidence of stones and the recurrence rate are still high, which may be related to the

Received: February 26, 2023
Accepted: June 29, 2023
Published: July 14, 2023

insufficient effectiveness of existing drugs.[12] Traditional anti-stone botanicals have the advantages of being cheap, safe, easy to obtain, and having diverse biological activities, and they may become an important source of anti-stone drugs.[13] Corn silk is a byproduct of corn crops, and many of its biological activities have been widely reported, including antioxidant activity, anti-diabetic activity, diuretic activity, and an antilithiasic effect.[14−17] However, the specific active ingredients of the antilithiasic effect of corn silk are still unclear. As one of the most important active ingredients in most plants, polysaccharides are currently attracting increasing attention from researchers. Plant polysaccharides are rich in anionic groups ($-COO^-$ and $-OSO_3^-$). They have a good ability to chelate calcium ions, provide cell protection, and have good potential for inhibiting the formation and recurrence of stones.

In our previous research,[18] corn silk polysaccharides (CSP) were extracted by hot water extraction, and carboxylate-modified CSP (CCSP) with different carboxyl contents were obtained. Based on the FT-IR, ^1H, and ^{13}C NMR detection results, the CSPs primarily consist of α-D-Glcp, α-L-Araf, α-L-Rhap, β-D-Galp, β-D-Manp, and β-D-Xylp. CCSP showed better antioxidant activity and could more effectively repair renal epithelial cells damaged by high oxalate than CSP. Whether CSP could directly regulate the interaction between CaOx crystals and cells, thereby affecting the cytotoxicity of the crystals, remains unclear. In the present study, whether CCSP could affect the toxic effects and endocytosis of nano-COM crystals was further explored to clarify the relationship between crystal endocytosis and cytotoxicity.

2. MATERIALS AND METHODS

2.1. Reagents and Apparatus. *2.1.1. Reagents.* Corn silk polysaccharide (CSP, polysaccharide content = 95%) was provided by Shaanxi Ciyuan Biotechnology Co., Ltd. Human kidney proximal tubular epithelial cells (HK-2) were purchased from the Shanghai Cell Bank of the Chinese Academy of Sciences (Shanghai, China). Fetal bovine serum and DMEM/F-12 cell culture medium were purchased from Gibco. 5,5′,6,6′-tetrachloro-1,1′,3,3′-tetraethylbenzimi-dazolylcarbocyanine iodide (JC-1) and Annexin V-FITC/PI Apoptosis Kit were purchased from KeyGEN BioTECH Co. Ltd. (Nanjing, China). Fluorescein isothiocyanate (FITC), Fluo-4 AM, DiI, 4,6-diamidino-2-phenyl indole (DAPI) staining solution, and paraformaldehyde were purchased from Beyotime Bio-Tech Co., Ltd. (Shanghai, China). Acridine orange (AO) and monodansylcadaverine (MDC) were purchased from Beijing Soleibao Technology Co., Ltd. (Beijing, China). Malondialdehyde (MDA) and superoxide dismutase (SOD) assay kits were purchased from Nanjing Jiancheng Bioengineering Institute (Nanjing, China). IgG-FITC secondary antibody was purchased from Wuhan Boster Bioengineering Co., Ltd. (Wuhan, China). The experimental water is double distilled water.

2.1.2. Instruments. Laser confocal microscope (LSM510 META DUO SCAN, ZEISS, Germany), inverted fluorescence microscope (Leica DMRA2, Germany), microplate reader (Gen5, Bio Tek, USA), flow cytometer (FACS Aria, BD, USA), scanning electron microscope (SEM, JSM-TE300), and optical microscope (OLYMPUS, CKX41, Japan).

2.2. Experimental Methods. *2.2.1. Preparation and Carboxylation of CSP.* Samples of corn silk were collected from the Shandong of China from July to September 2021. The material was sorted, washed, and dried immediately by forced air circulation at 50−60 °C. The polysaccharide content was 95%. CSPs were obtained from corn silk by a hot water-extracted method.

The original corn silk polysaccharide (CSP0) was carboxymethylated according to our previous method,[19] three carboxymethylated corn silk polysaccharides (CCSP1, CCSP2, and CCSP3) were obtained. The −COOH content of polysaccharides was determined by the conductivity titration method. The −COOH content of CSP0, CCSP1, CCSP2, and CCSP3 was 3.92, 7.75, 12.90, and 16.38%, respectively.

2.2.2. Preparation and Fluorescent Labeling of Nano-COM. Nano-sized COM crystals with a size of about 100 nm were prepared according to our previous study.[20] $CaCl_2$ and K_2Ox water solutions were prepared with a concentration of 0.60 mol/L. 50 mL of each solution was directly mixed at room temperature. The reaction mixture was stirred with a magnetic stirrer for 6 min; then, ethanediol was added to promote the precipitation. The characterization results of X-ray diffraction, Fourier transform infrared spectroscopy, and SEM show that they were all target crystals. The nano-COM was fluorescently labeled with FITC according to the method reported by Zhao et al.[21]

2.2.3. Cell Culture and Grouping. HK-2 cells were grown in DMEM/F-12 medium supplemented with 10% fetal bovine serum and penicillin−streptomycin antibiotics at 37 °C under an atmosphere of 95% air and 5% CO_2. The experimental models were divided into three groups: (A) normal control group (NC): only serum-free medium was added; (B) COM treatment group: 200 μg/mL nano-COM dispersed in serum-free medium was added and co-incubated with cells for 12 h; (C) CCSPs protection group: a certain concentration of CCSPs (CSP0, CCSP1, CCSP2, and CCSP3) with different carboxyl content mixed with 200 μg/mL COM crystals were added to the cells and co-incubated with cells for 12 h.

2.2.4. Cell Morphology Observation. HK-2 cells were seeded into 12-well plates at a density of 1.0×10^5 cells/mL and cultured for 24 h. 200 μg/mL nano-COM crystals with or without the protection of 60 μg/mL CCSPs (CSP0, CCSP1, CCSP2, and CCSP3) were added and co-incubated with cells for 12 h. After reaching the treatment time, cell morphology was observed under an ordinary optical microscope.

2.2.5. Observation of Crystal Endocytosis by Confocal Microscopy. The FITC-labeled nano-COM (200 μg/mL) with or without the protection of 60 μg/mL CCSPs (CSP0, CCSP1, CCSP2, and CCSP3) were added and co-incubated with cells for 12 h. After reaching the treatment time, 5 mM ethylenediaminetetraacetic acid (EDTA) was treated for 10 min to remove the adherent crystals, and 500 μL of DiI was added for staining for 10 min. The nuclei were stained with DAPI and fixed with 4% paraformaldehyde for 10 min. The internalized crystals and cell morphology were observed by a laser confocal microscope.

2.2.6. Quantitative Detection of the Proportion of Cells with Endocytosed Crystals. The FITC-labeled nano-COM (200 μg/mL) with or without the protection of 60 μg/mL CCSPs (CSP0, CCSP1, CCSP2, and CCSP3) were added and co-incubated with cells for 12 h. After reaching the treatment time, 5 mM ethylenediaminetetraacetic acid (EDTA) was treated for 10 min to remove the adherent crystals. The cells were collected and resuspended in PBS, and the proportion of fluorescent cells was detected by flow cytometry.

2.2.7. Detection of Lysosome Integrity. The cells were stained with 5 μg/mL acridine orange (AO) for 15 min, and

https://doi.org/10.1021/acsomega.3c01306
ACS Omega 2023, 8, 25839−25849

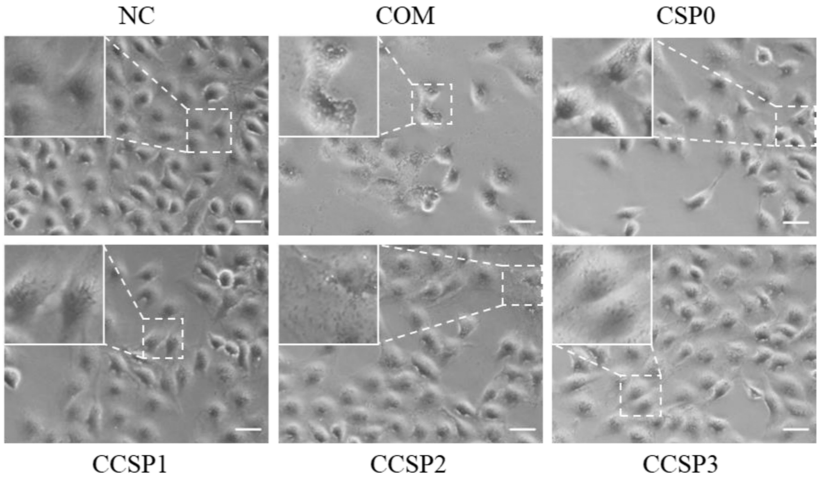

Figure 1. Changes in cell morphology of HK-2 cells after the treatment of nano-COM crystals with or without protection by CSPs (CSP0, CCSP1, CCSP2, and CCSP3) for 12 h. COM concentration: 200 μg/mL. CSPs concentration: 60 μg/mL. Scale bars: 50 μm.

the cells were washed three times with PBS. Then, 200 μg/mL nano-COM crystals with or without protection by 60 μg/mL CCSPs (CSP0, CCSP1, CCSP2, and CCSP3) were added and co-incubated with cells for 12 h. After reaching the treatment time, the cells were washed three times with PBS, and the integrity of the lysosome was observed under a fluorescence microscope.

2.2.8. Detection of the Intracellular Ca^{2+} Level. 200 μg/mL nano-COM crystals with or without protection by 60 μg/mL CCSPs (CSP0, CCSP1, CCSP2, and CCSP3) were added and co-incubated with cells for 12 h. After reaching the treatment time, the treated cells were washed twice with PBS, incubated with 2 μM Fluo-4 AM in the dark for 45 min, and then stained with DAPI for 10 min. The intracellular Ca^{2+} level in the treated cells was observed with a laser confocal microscope and quantitatively detected by a flow cytometer.

2.2.9. Detection of Mitochondrial Membrane Potential ($\Delta\Psi m$). 200 μg/mL nano-COM crystals with or without protection by 60 μg/mL CCSPs (CSP0, CCSP1, CCSP2, and CCSP3) were added and co-incubated with cells for 12 h. After reaching the treatment time, the supernatant was aspirated into the culture plate, and 1 mL of JC-1 working solution was added. The cells were incubated in a 37 °C incubator in the dark for 30 min, washed twice with PBS, and observed with an inverted fluorescence microscope. ImageJ software was used to perform fluorescence semi-quantitative analysis.

2.2.10. Detection of SOD and MDA Levels in Cells. 200 μg/mL nano-COM crystals with or without protection by 60 μg/mL CCSPs (CSP0, CCSP1, CCSP2, and CCSP3) were added and co-incubated with cells for 12 h. After reaching the action time, the treated cells are tested with the SOD kit and the MDA kit according to the kit instructions.

2.2.11. Detection of Autophagy. 200 μg/mL nano-COM crystals with or without protection by 60 μg/mL CCSPs (CSP0, CCSP1, CCSP2, and CCSP3) were added and co-incubated with cells for 12 h. After the incubation time was reached, the culture solution was removed and washed twice with 1× wash buffer, and 1 mL of 10% monodansylcadaverine (MDC) dye was added to each well and incubated in an incubator in the dark for 30 min. The autophagy level was observed and tested by a fluorescence microscope and a flow cytometer.

2.2.12. Detection of Apoptosis and Necrosis. 200 μg/mL nano-COM crystals with or without protection by 60 μg/mL CCSPs (CSP0, CCSP1, CCSP2, and CCSP3) were added and co-incubated with cells for 12 h. The cells were collected and washed with PBS (centrifuged at 1000 rpm for 5 min). 5 μL annexin V-FITC and 5 μL PI were added and then incubated in darkness at room temperature for 10 min. The prepared cells were then analyzed using flow cytometry.

2.2.13. Statistical Analysis. Statistical analyses were performed using SPSS 13.0 software. The Data were expressed as mean ± SD. Multiple group comparisons were performed using one-way ANOVA, followed by the Tukey post hoc test.

3. RESULTS

3.1. CCSPs Inhibit the Destruction of Cell Morphology. In our previous study,[19] we explored the repair effect of carboxymethyl-modified corn silk polysaccharide (CSP) on oxidatively damaged renal epithelial cells. CCSPs had no toxicity to HK-2 cells at a concentration range of 20−100 μg/mL for 12 h. CCSPs showed the best bioactivity at a concentration of 60 μg/mL.

Original CSP (CSP0), carboxymethylated CSP (CCSP1, CCSP2, and CCSP3, 60 μg/mL), and 200 μg/mL nano-COM crystals were co-cultured with HK-2 cells for 12 h. Changes in cell morphology were observed by an ordinary optical microscope (Figure 1). The normal group showed full cell morphology and tight connections between cells. The nano-COM crystal damage group without polysaccharide protection had a large number of crystals attached to the surface (enlarged image in the upper left corner). The cell morphology was abnormal, the number of cells was reduced, and the distribution of cells was loose. Under the protection of CCSPs with different carboxyl contents (3.92, 7.75, 12.90, and 16.38%), as the content of −COOH in the polysaccharides increased, the cells gradually became fuller, the attached crystals on the cell surface gradually decreased, the cells became denser, and the overall cell morphology gradually improved.

3.2. Nano-COM Crystals Distribution in Cells. DiI and DAPI were used to fluorescently stain the cell membrane and nucleus. Nano-COM was fluorescently labeled with fluorescein isothiocyanate (FITC). The adhered COM crystals were removed via complexation and dissolution with 5 mM EDTA.

https://doi.org/10.1021/acsomega.3c01306
ACS Omega 2023, 8, 25839−25849

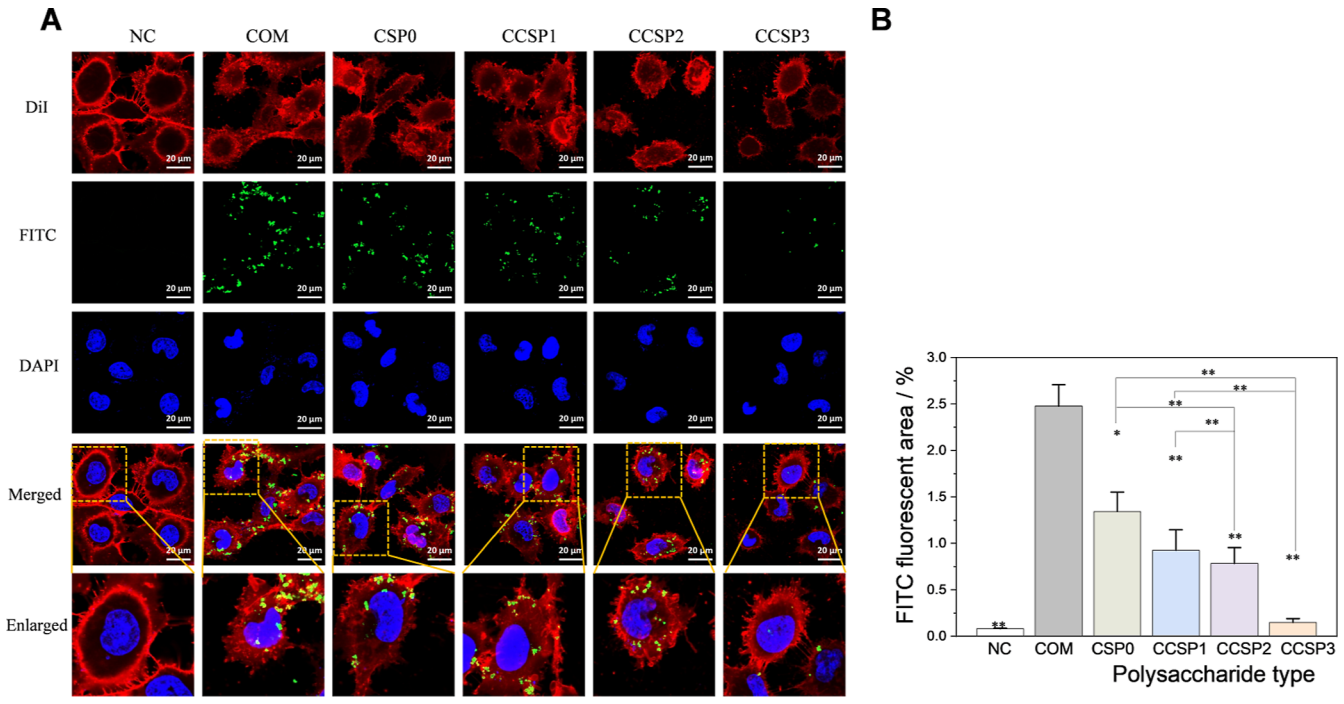

Figure 2. Observation of COM crystal endocytosis by laser scanning confocal microscopy. Cell membrane (red fluorescence), nucleus (blue fluorescence), and COM crystals (green fluorescence). (A) Fluorescence microscope image and (B) quantitative histogram of green fluorescence intensity. COM concentration: 200 μg/mL. CSPs concentration: 60 μg/mL. Protection time: 12 h. Compared with the COM treatment group, $^{*}P < 0.05$ and $^{**}P < 0.01$. Scale bars: 20 μm.

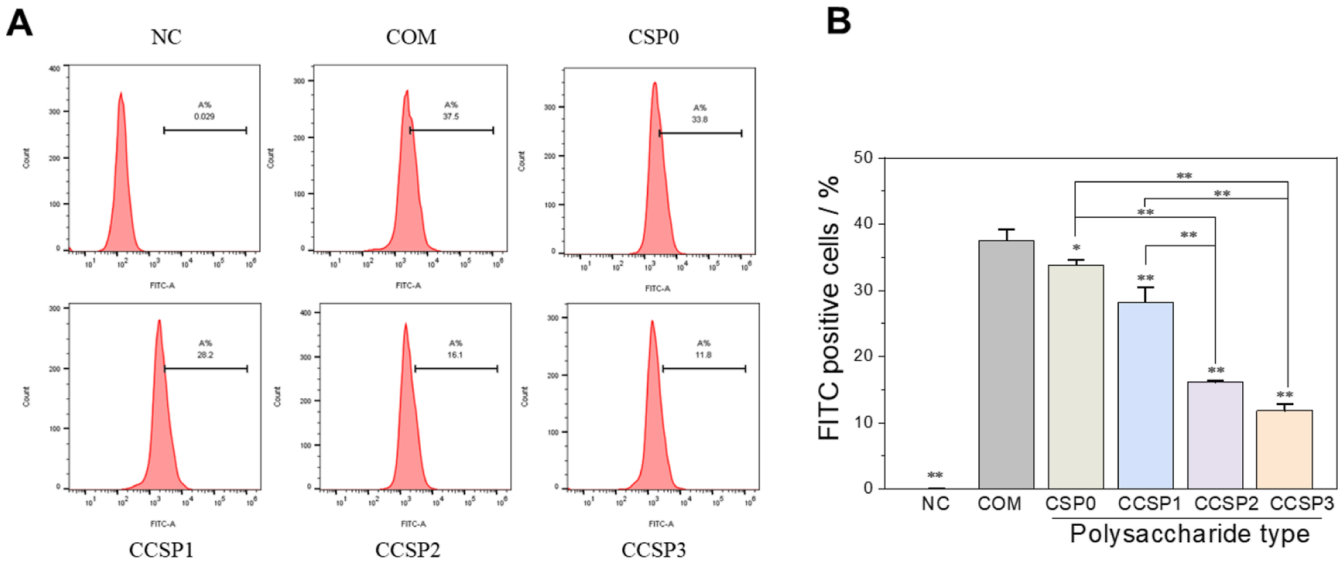

Figure 3. Changes in the proportion of cells with internalized crystals after the treatment of nano-COM crystals with or without the protection of CSPs (CSP0, CCSP1, CCSP2, and CCSP3) for 12 h. (A) Quantitative detection of the proportion of cells with internalized crystals by flow cytometry; (B) quantitative histogram of the proportion of cells with internalized crystals. COM concentration: 200 μg/mL. CSPs concentration: 60 μg/mL. Protection time: 12 h. Compared with the COM treatment group, $^{*}P < 0.05$, $^{**}P < 0.01$.

The internalized crystals were detected via laser scanning confocal microscopy (Figure 2). In the CCSP-unprotected cells, nano-COM crystals caused the cell morphology to become irregular and the cell membrane to become blurred. A large number of crystals accumulated in the cell, and the aggregation was serious. In the CCSP-protected cells, the number of endocytosed crystals was obviously less than that in the unprotected group, and the degree of crystal aggregation was reduced. The CCSP3 with the highest −COOH content exhibited the best inhibition ability for crystal internalization.

3.3. Quantitative Detection of Endocytosed Nano-COM Crystals. Flow cytometry was used to quantitatively detect the proportion of cells that had endocytosed crystals in each group (Figure 3). The detected FITC-positive cells were the cells with internalized crystals. In the CCSP-unprotected group, the proportion of cells that endocytosed crystals was the largest (37.5%). Under the protection of CCSPs, as the

https://doi.org/10.1021/acsomega.3c01306
ACS Omega 2023, 8, 25839−25849

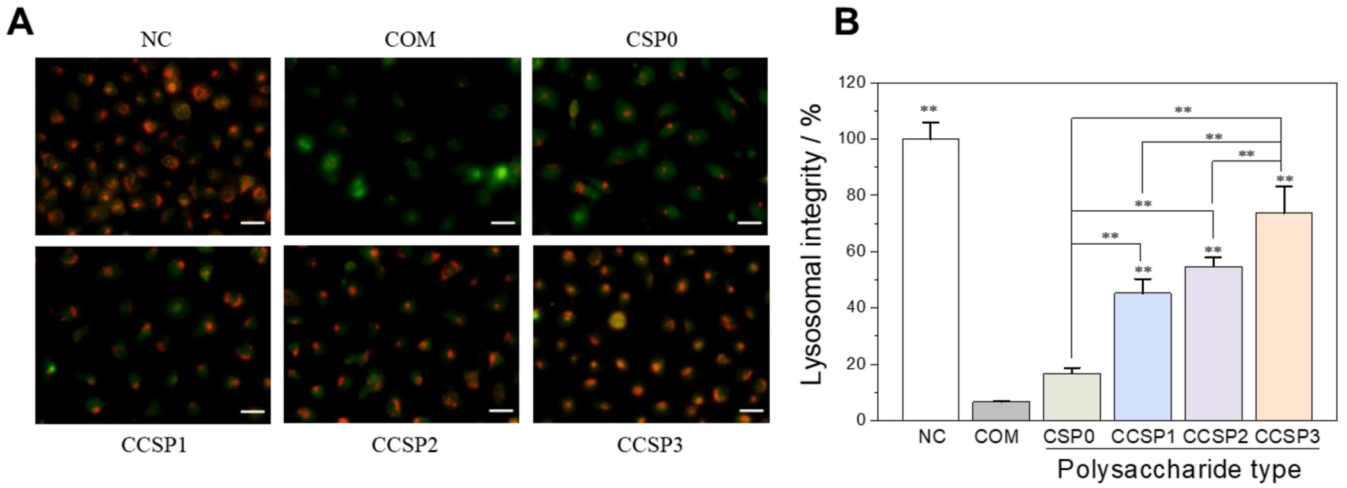

Figure 4. Changes of lysosomal integrity of HK-2 cells after the treatment of nano-COM crystals with or without the protection of CSPs (CSP0, CCSP1, CCSP2, and CCSP3) for 12 h. (A) Lysosomal integrity was observed by fluorescence microscopy; (B) quantitative histogram of lysosomal integrity. COM concentration: 200 μg/mL. CSPs concentration: 60 μg/mL. Protection time: 12 h. Compared with the COM treatment group, $^{*}P < 0.05$ and $^{**}P < 0.01$. Scale bars: 50 μm.

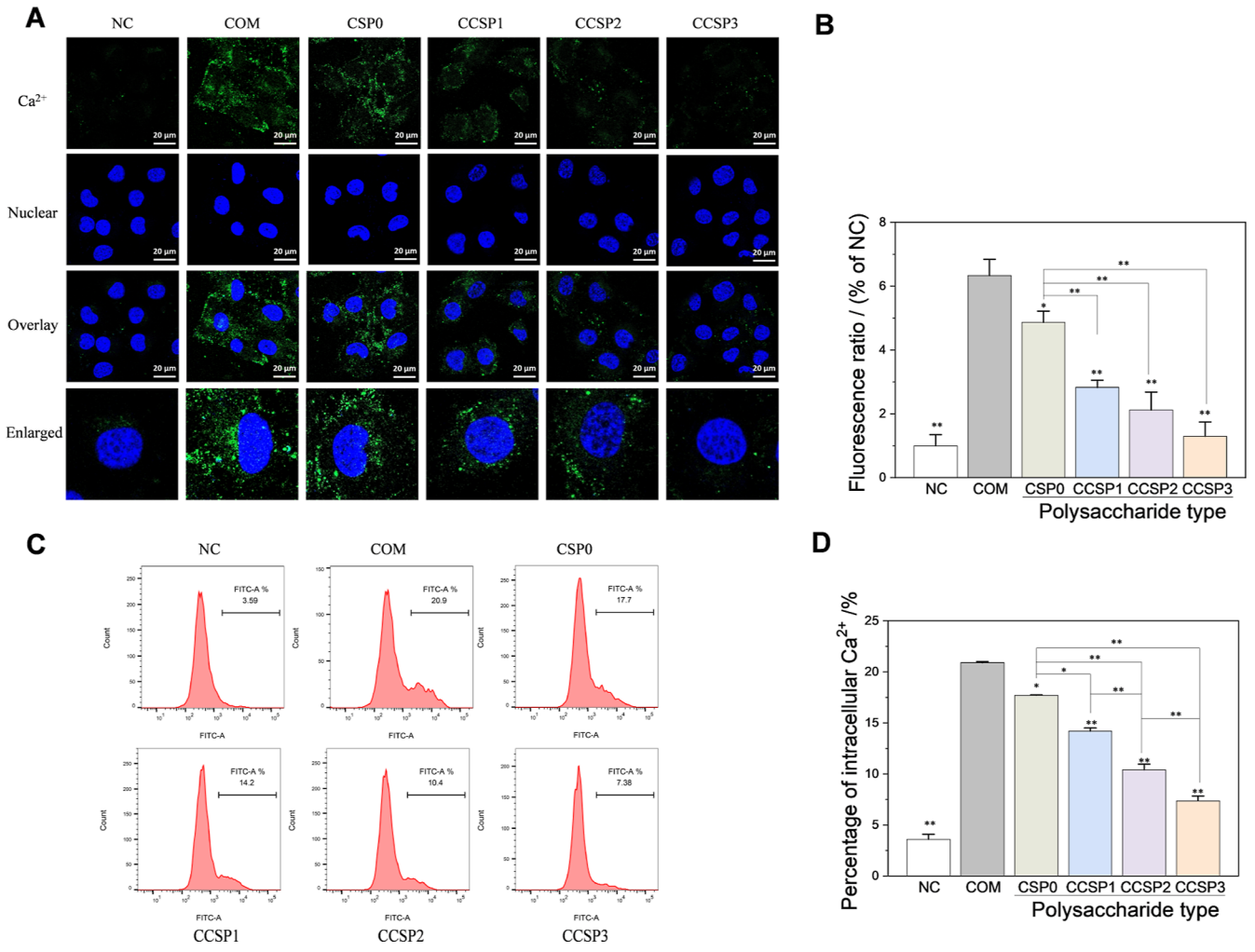

Figure 5. Changes of intracellular Ca^{2+} levels of HK-2 cells after the treatment of nano-COM crystals with or without the protection of CSPs (CSP0, CCSP1, CCSP2, and CCSP3) for 12 h. (A) Ca^{2+} levels were observed by fluorescence microscopy; (B) quantitative histogram of green fluorescence intensity; (C) intracellular Ca^{2+} levels detected by flow cytometry; (D) quantitative histogram of Ca^{2+} level. COM concentration: 200 μg/mL. CSPs concentration: 60 μg/mL. Protection time: 12 h. Compared with the COM treatment group, $^{*}P < 0.05$ and $^{**}P < 0.01$. Scale bars: 20 μm.

https://doi.org/10.1021/acsomega.3c01306
ACS Omega 2023, 8, 25839−25849

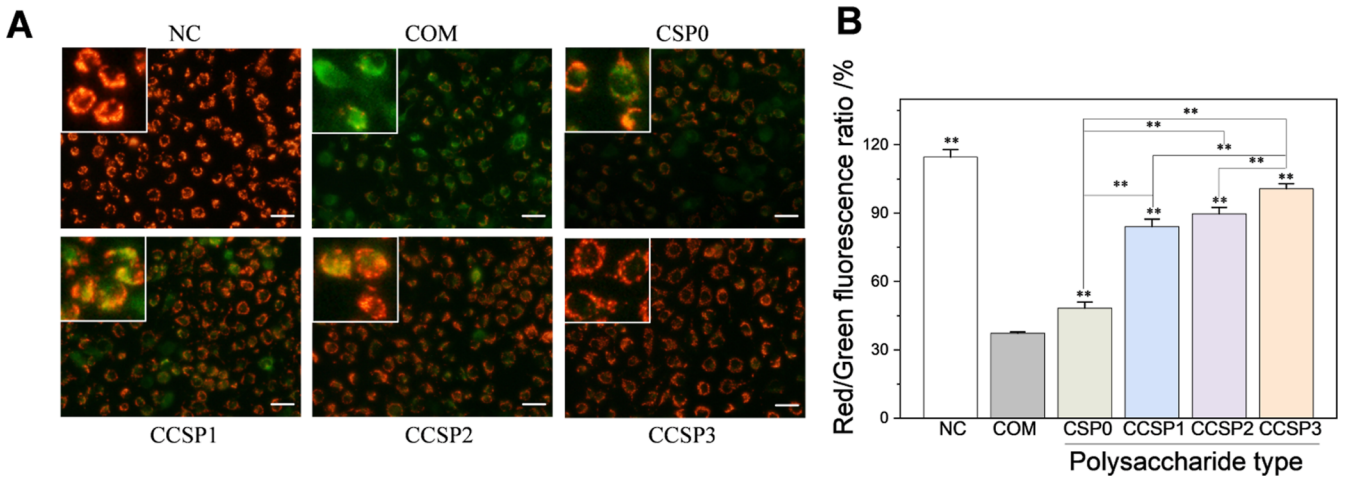

Figure 6. Changes of mitochondrial membrane potential (ΔΨm) of HK-2 cells after the treatment of nano-COM crystals with or without the protection of CSPs (CSP0, CCSP1, CCSP2, and CCSP3) for 12 h. (A) Visualization of ΔΨm observed by fluorescence microscopy. (B) Quantitative result of ΔΨm. COM concentration: 200 μg/mL. CSPs concentration: 60 μg/mL. Protection time: 12 h. Compared with the COM treatment group, $^{*}P < 0.05$ and $^{**}P < 0.01$. Scale bars: 50 μm.

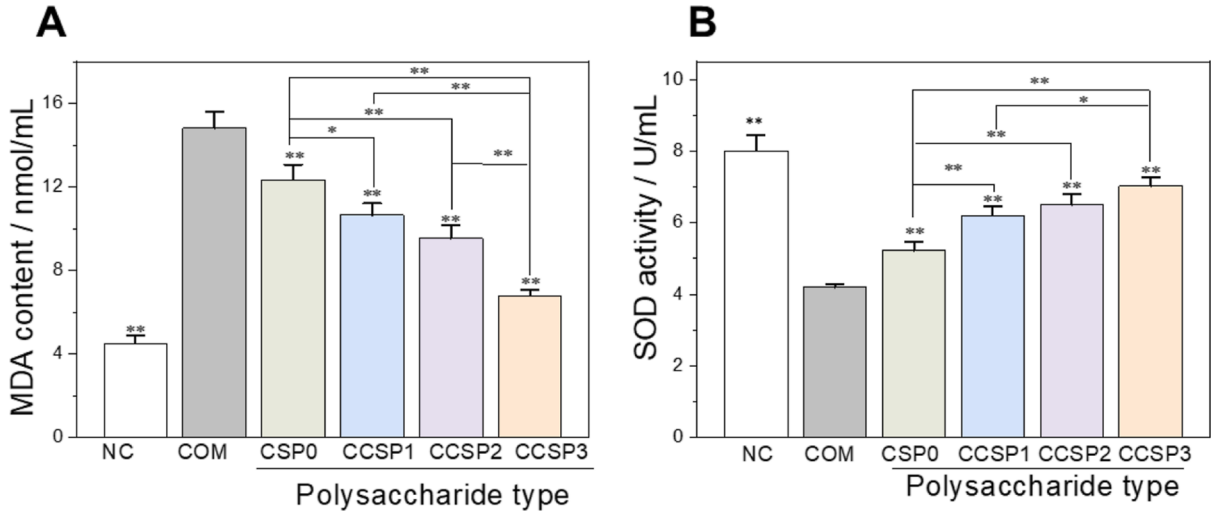

Figure 7. Change of malondialdehyde (MDA) levels and superoxide dismutase (SOD) activities of HK-2 cells after the treatment of nano-COM crystals with or without protection by CSPs (CSP0, CCSP1, CCSP2, and CCSP3) for 12 h. (A) MDA content; (B) SOD activity. COM concentration: 200 μg/mL. CSP concentration: 60 μg/mL. Protection time: 12 h. Compared with the COM treatment group, $^{*}P < 0.05$ and $^{**}P < 0.01$. Scale bars: 50 μm.

content of −COOH in CCSPs increased, the proportion of FITC-positive cells gradually decreased, that is, the number of endocytic crystals gradually decreased. This finding showed that CCSPs inhibited the endocytosis of nano-COM, and the inhibitory effect was in the following order: CSP0 < CCSP1 < CCSP2 < CCSP3.

3.4. CCSPs Inhibit Lysosomal Rupture. The interior of the lysosome is acidic with a pH around 4.8, and the cytoplasm is neutral with a pH around 7.0. Acridine orange (AO) is a pH-responsive fluorescent probe that exhibits red fluorescence in lysosomes and green fluorescence in the cytoplasm.[22] As shown in Figure 4, the lysosomes in a normal cell were in good integrity, and the superposition of red fluorescence and green fluorescence showed more orange fluorescence. After COM crystal damage for 12 h, red fluorescence was obviously weakened, indicating that the structure of lysosomes was seriously damaged. Under the protection of CCSPs, with the increase in −COOH content, the red fluorescence gradually increased, and the degree of lysosome damage decreased. Thus, CCSPs could inhibit the destruction of lysosomal integrity caused by COM crystals and reduce the damage of COM to cells.

3.5. CCSPs Reduce Intracellular Ca^{2+} Levels. The fluorescent probe Fluo-4 AM was used to fluorescently label the intracellular Ca^{2+}.[23] The intracellular Ca^{2+} levels before and after the protection of each CCSPs were observed with a laser confocal microscope (Figure 5A,B). The green fluorescence of normal cells was weak. After nano-COM damage, the green fluorescence of cells became strong. Under the protection of each CCSP, as the content of −COOH in CCSPs increased, the green fluorescence gradually weakened. Thus, CCSPs could inhibit the increase in Ca^{2+} levels caused by nano-COM. CCSP3, with the highest −COOH content (16.38%), demonstrated the best suppression effect.

In addition, the fluorescence intensity of Ca^{2+} was quantitatively detected using a flow cytometer (Figure

https://doi.org/10.1021/acsomega.3c01306
ACS Omega 2023, 8, 25839−25849

5C,D). The intracellular Ca^{2+} ratio of the nano-COM treatment group (20.9%) was significantly higher than that of the normal cell group (3.59%, $P < 0.01$). The level of Ca^{2+} in the CCSP protection group gradually decreased with the increase in −COOH content in the polysaccharide (7.38−17.7%). Thus, CCSPs could inhibit the increase in Ca^{2+} level caused by nano-COM, and the inhibitory effect was as follows: CSP0 < CCSP1 < CCSP2 < CCSP3.

3.6. CCSPs Increase Mitochondrial Membrane Potential. The JC-1 fluorescent probe was used to fluorescently label the mitochondrial membrane potential in the cell.[24] The mitochondria in normal cells are usually in a high membrane potential state, and they show red fluorescence. When the mitochondria are damaged, the membrane potential drops and shows green fluorescence. As shown in Figure 5, cells in the normal group demonstrated strong red fluorescence, indicating that their mitochondrial membrane potential was high. The cells in the nano-COM injury group showed weak red fluorescence, mainly showing green fluorescence; that is, the membrane potential of the injury group was obviously reduced. Under the protection of CCSPs, the red fluorescence of the cells gradually increased with the increase in the −COOH content in the polysaccharide. Thus, CCSPs could protect HK-2 cells and reduce mitochondrial damage caused by nano-COM.

3.7. CCSPs Improve the Antioxidant Capacity of Cells. The release amount of malondialdehyde (MDA) is a commonly used index indicating the degree of lipid peroxidation damage in cells.[25] Superoxide dismutase (SOD) is the main antioxidant enzyme in the cell. It can scavenge free radicals in the body and resist the damage caused by free radicals to the organism. In this study, MDA and SOD detection kits were used to detect the release of MDA (Figure 7A) and the activity of the SOD enzyme (Figure 7B) in the cell, respectively, before and after CCSP protection. After the cells were treated with nano-COM crystals for 12 h, the MDA content increased from 4.50 nmol/mL in the control group to 14.82 nmol/mL, and the SOD enzyme activity decreased from 5.84 to 3.35 U/mL. Under the protection of CCSP3, the MDA content decreased to 6.78 nmol/mL, and the SOD enzyme activity increased to 7.03 U/mL. Thus, CCSPs could inhibit the increase in MDA release and the decrease in SOD enzyme activity caused by nano-COM crystals, reduce lipid peroxidation damage, and improve the ability of cells to resist free radicals. The higher the −COOH content of CCSPs, the better the effect of antioxidant capacity.

3.8. CCSP Inhibit Autophagy. Autophagy is the process of engulfing one's own cytoplasmic proteins or organelles, coating them into vesicles, fusing with lysosomes to form autophagic lysosomes, and degrading the contents it encapsulates.[26] Monodansylcadaverine (MDC) is an autofluorescent compound that can specifically label autophagic vesicles. In the present study, HK-2 cells were stained with MDC, and flow cytometry and fluorescence microscopy were used to detect the level of autophagy in the cells (Figure 8). In the normal group, the blue fluorescence intensity was weak, and the proportion of MDC-positive cells was the lowest (3.72%). The blue dot-like fluorescence in the cells of the nano-COM injury group was obviously increased, and the proportion of MDC-positive cells was 27.9%. Under the protection of CCSPs with different degrees of carboxylation, with the increase in −COOH content, the proportion of positive cells gradually decreased. These results showed that CCSPs could inhibit autophagy caused by nano-COM, and the higher the −COOH content, the better the inhibitory effect.

3.9. CCSPs Inhibit Cell Apoptosis and Necrosis. The annexin V-FITC/PI double staining method was used to detect the proportion of apoptosis and necrotic cells (Figure 9).[27] The proportion of dead cells in the normal cell group was 9.80%. The apoptosis and necrosis rates of the nano-COM injury group without CCSP protection were obviously increased, and the proportion of dead cells increased to 39.3%, of which necrotic cells were the main ones (33.5%). Under the protection of CCSPs, the number of dead cells was obviously reduced (35.8−16.1%), and it gradually decreased with the increase in the −COOH content of CCSPs.

4. DISCUSSION

4.1. CCSPs Inhibit the Accumulation of Nano-COM in Cells. In our previous study,[18] we demonstrated that CSPs can regulate CaOx crystallization. CCSPs can interact with the surface of COM crystals through a calcium bridge, which prevents free Ca^{2+} from penetrating into the lattice of COM, thus inhibiting the formation of COM crystals. The −COOH groups in CSPs can increase the enrichment of Ca^{2+} on the polysaccharide surface and form a high-energy interface on the polysaccharide surface. Both high-energy interfaces and high calcium energy states can promote thermodynamically metastable COD formation.

In addition, the interaction (adhesion and endocytosis) between crystals and renal tubular epithelial cells is an important process in stone formation.[28] The damage to renal tubular epithelial cells could promote the retention of crystals on the cell surface.[29] The rapid endocytosis of a small number of attached crystals by epithelial cells is a protective mechanism to eliminate residual crystals.[30] COM crystals can be endocytosed into intracellular lysosomes through the transport function and dissolved under the action of hydrolase in the lysosomes to release Ca^{2+} and Ox^{2-}. Too many crystals that are endocytosed, exceeding the digestive capacity of the cell itself, could cause the rupture of the lysosome and cell damage.[31]

CCSPs are anionic polysaccharides rich in −COOH groups.[18] They could interact with nano-COM and increase the negative charge on the surface of the COM crystal. As the content of −COOH in CCSPs increased, the negative charge of the COM crystal increased. The surface of renal epithelial cells generally has a certain negative charge, and as the damage worsens, the negative charge on the cell surface increases. The adsorption of CCSPs on the surface of nano-COM increases the repulsive force between the crystal and the negatively charged cell membrane, inhibits the adhesion between the crystal and the cell, and thus inhibits the endocytosis of the crystal by the cell.[32]

In addition to crystal−cell interactions, CaOx is also affected by other factors, such as urea and carbon dioxide. The presence of urea and carbon dioxide in the kidney system can affect the pH of urine and blood, thereby affecting the formation and growth of CaOx crystals and increasing the risk of CaOx stone formation.[33]

4.2. CCSPs Inhibit Oxidative Damage of Cells Caused by Nano-COM. The endocytosed nano-COM crystals dissolved under the action of hydrolase in the lysosome, releasing a large amount of Ox^{2-} and Ca^{2+} (Figure 5). The release of a large amount of Ca^{2+} could cause an imbalance in the level of Ca^{2+} inside and outside the cell, causing an intracellular stress response. The cycling of calcium ions in the

https://doi.org/10.1021/acsomega.3c01306
ACS Omega 2023, 8, 25839−25849

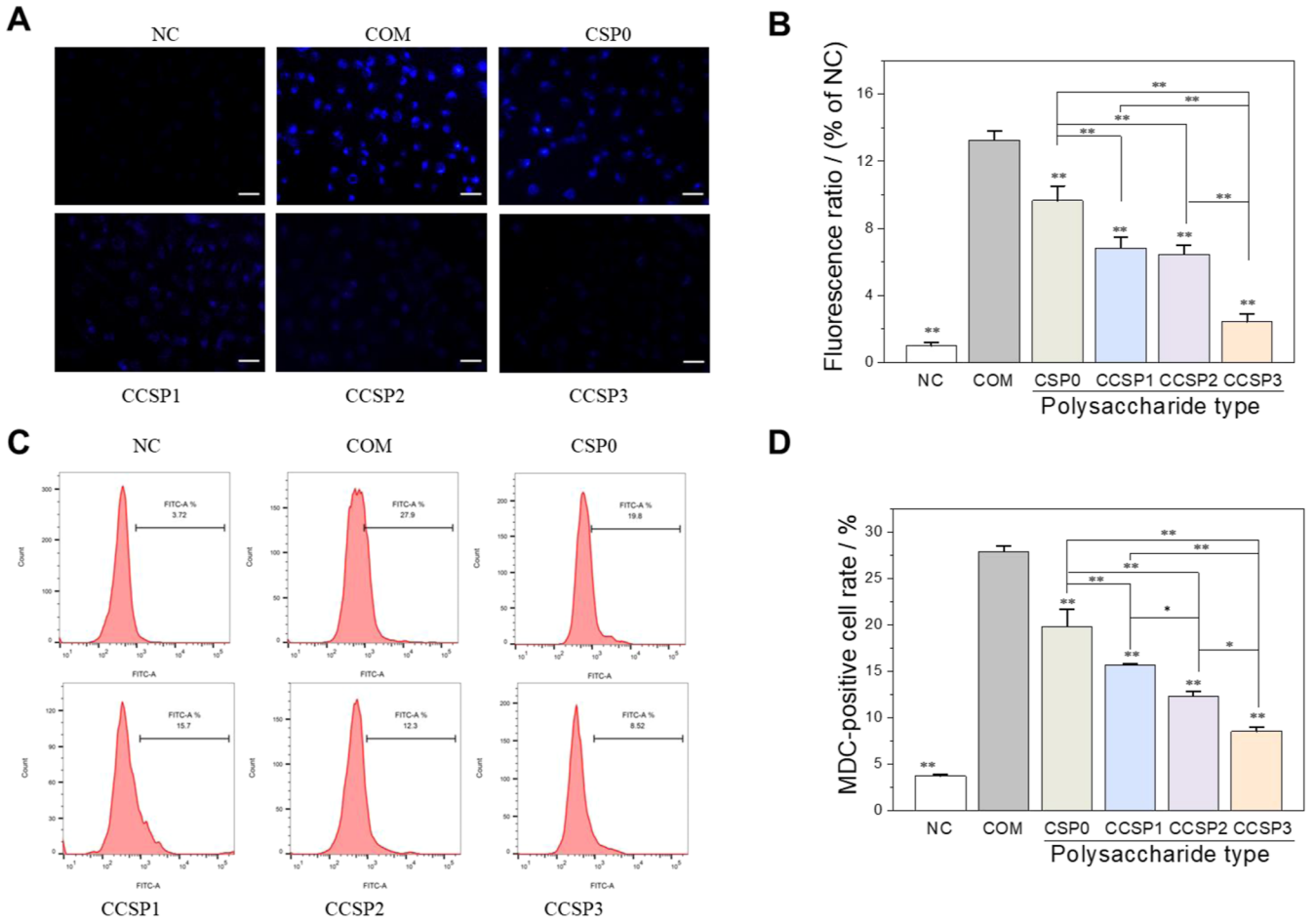

Figure 8. SLPs inhibit autophagy of HK-2 cells after the treatment of nano-COM crystals with or without the protection of CSPs (CSP0, CCSP1, CCSP2, and CCSP3) for 12 h. (A) Fluorescence microscope image; (B) quantitative histogram of MDC fluorescence intensity; (C) flow cytometry quantitative detection of autophagy level; (D) quantitative histogram of autophagy levels. COM concentration: 200 μg/mL. CSPs concentration: 60 μg/mL. Protection time: 12 h. Compared with the COM treatment group, $^{*}P < 0.05$ and $^{**}P < 0.01$. Scale bars: 50 μm.

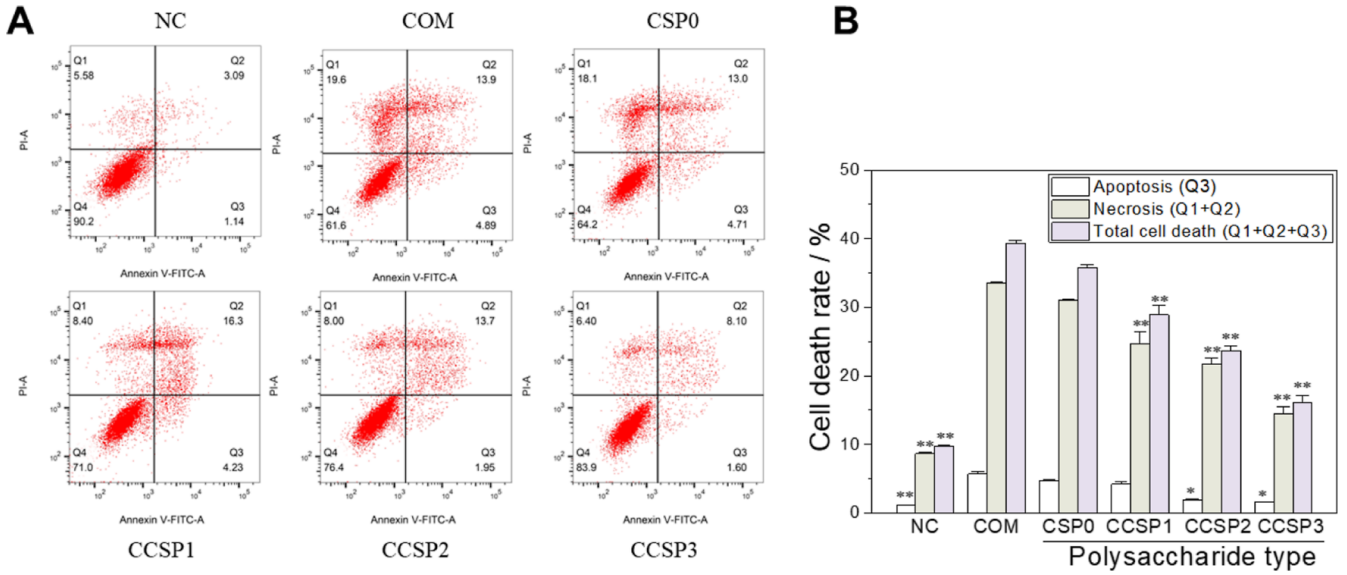

Figure 9. Changes in cell death rate of HK-2 cells after the treatment of nano-COM crystals with or without the protection of CSPs (CSP0, CCSP1, CCSP2, and CCSP3) for 12 h. (A) Quantitative detection of cell apoptosis and necrosis by Annexin V/PI double staining. Quadrants Q1, Q2, Q3, and Q4 denote the ratio of necrotic cells, late-stage apoptotic cells, early-stage apoptotic cells, and normal cells, respectively; (B) quantitative histogram of cell apoptosis and necrosis rates. COM concentration: 200 μg/mL. CSPs concentration: 60 μg/mL. Protection time: 12 h. Compared with the COM treatment group, $^{*}P < 0.05$, $^{**}P < 0.01$.

https://doi.org/10.1021/acsomega.3c01306
ACS Omega 2023, 8, 25839−25849

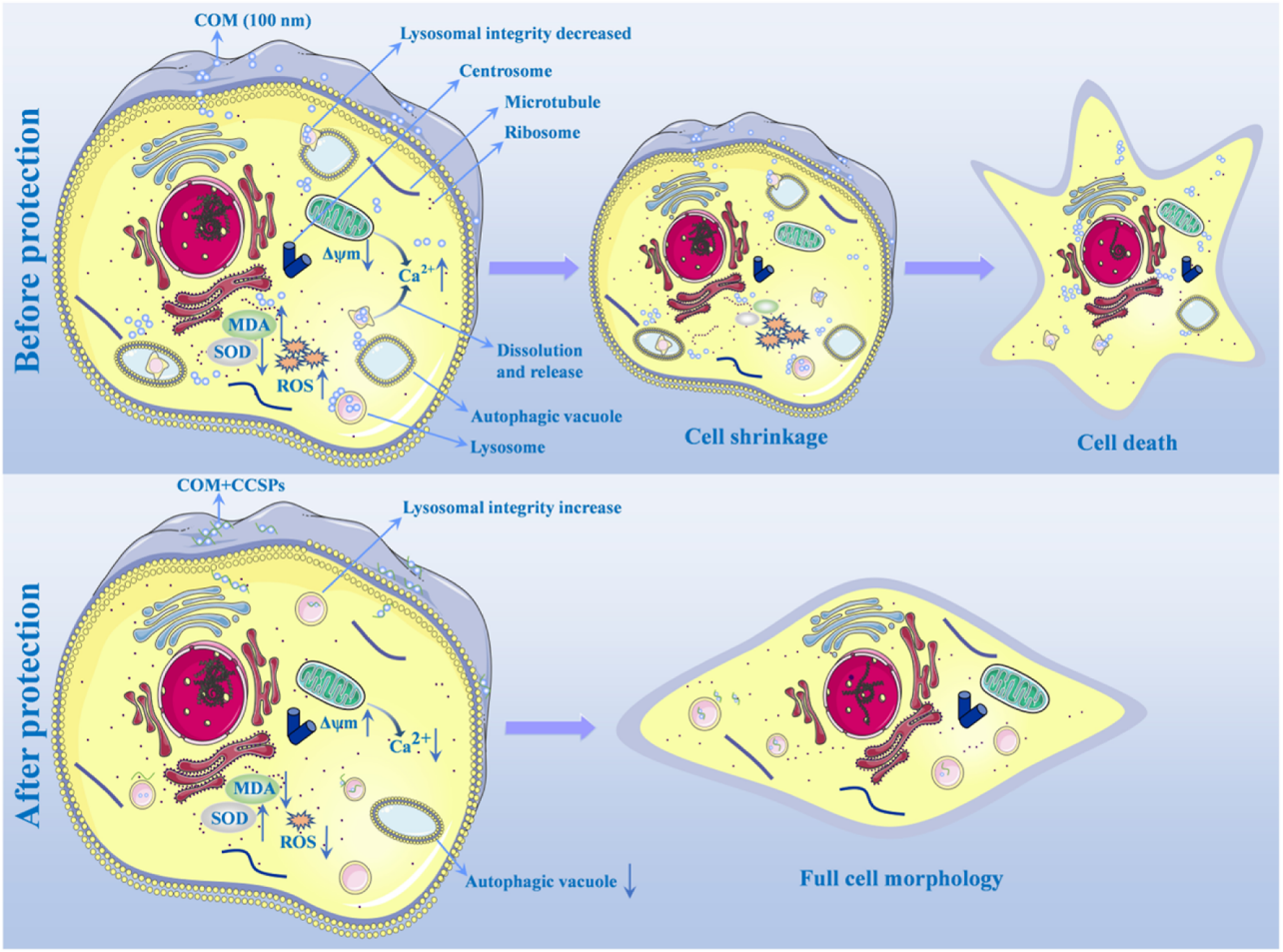

Figure 10. Proposed schematic illustration of CSPs protecting HK-2 cells against nano-COM crystal damage and inhibiting crystal endocytosis.

kidney involves three stages: filtration after intestinal absorption, reabsorption, and excretion. The calcium ion is one of the essential ions required for cell signaling and cell proliferation. In the process of formation and development of renal tubular epithelial cells, calcium ions can regulate cell proliferation and differentiation and participate in the formation of cell membranes and the cytoskeleton. Too much Ca^{2+} can have toxic effects on cells and even cause cell death.[34,35] Ca^{2+} overload has even been suggested to be the final common pathway of all types of cell death.

Nano-COM caused an increase in the MDA level of HK-2 cells and a decrease in SOD enzyme activity (Figure 8), which caused an imbalance between intracellular oxidation and antioxidation, resulting in cell oxidative damage. In addition, the endocytosed nano-COM crystals caused a decrease in the mitochondrial membrane potential (Figure 6). The increase in Ca^{2+} levels and lipid peroxidation may be important causes of mitochondrial damage.[36] Mitochondria are the main intracellular source of ROS, and mitochondrial metabolic disorders are accompanied by the production of ROS.[37] In addition, autophagy has been shown to be critical for the regulation of oxidative stress-induced renal tubular injury.[38] Nano-COM caused the enhancement of cell autophagy (Figure 8), which further aggravated cell damage. The interaction between crystals and cells caused oxidative stress damage to cells, which promoted the retention of crystals in the kidney and increased the risk of stone formation.[39]

In addition, CSPs are rich in −COOH groups, which have the effect of improving the cell's own antioxidant capacity, thereby resisting cell oxidative damage caused by nano-COM. In our previous study,[18] CSPs were found to have a good antioxidant capacity. A series of in vitro antioxidant experiments revealed that CCSPs can chelate ferrous ions and inhibit the Fenton reaction and free radical reaction, thus reducing oxidative stress levels and oxidative damage. CCSPs could improve the antioxidant capacity of cells, maintain cell morphology (Figure 1) and lysosome integrity (Figure 4), reduce intracellular autophagy (Figure 8) and Ca^{2+} levels (Figure 5), increase the mitochondrial membrane potential (Figure 6), and finally inhibit cell death (Figure 9). The degree of substitution (DS) of active groups is an important factor affecting the biological activity of natural polysaccharides.[40] In general, the higher the content of the sulfuric acid group ($-OSO_3^-$) or carboxyl group ($-COO^-$) in polysaccharides, the stronger its ability to reduce the loss of negative charges on the cell surface and protect the charge barrier, and the greater its ability to protect cells.[41,42] In the present study, carboxylated CCSPs with −COOH contents of 3.92, 7.75, 12.90, and 16.38% were used to protect HK-2 cells. The CCSPs with higher −COOH content showed better protection abilities.

The mechanism by which CCSPs inhibit nano-COM endocytosis and reduce the oxidative damage caused by crystals is shown in Figure 10. CCSPs were adsorbed on the surface of nano-COM crystals to increase the electrostatic

https://doi.org/10.1021/acsomega.3c01306
ACS Omega 2023, 8, 25839−25849

repulsion between the crystals and cells, inhibit the endocytosis of the crystals, reduce the enrichment of COM crystals in cells, and thus inhibit the damage of renal epithelial cells. In addition, CCSPs are rich in −COOH groups. They also have the effect of improving the cell's own antioxidant capacity, thereby resisting cell oxidative damage caused by nano-COM. Taken together, CCSPs inhibited the cell damage caused by the crystals by inhibiting the endocytosis of nano-COM crystals and increasing the antioxidant capacity of cells.

5. CONCLUSIONS

This study investigated the protective effects of CCSPs with different carboxyl contents (3.92, 7.75, 12.90, and 16.38%) on cell damage induced by nano-COM crystals. Nano-COM could induce the destruction of cell morphology and lysosome integrity, increase the level of intracellular Ca^{2+} and autophagy, reduce the activity of SOD, increase the MDA level, and increase cell apoptotic and necrotic rates. CCSPs reduced the damage caused by crystals by inhibiting the endocytosis of nano-COM by cells, of which CCSP3 with the highest −COOH content showed the best inhibition ability. Thus, these findings implied the potential clinical application of CCSPs for the prevention of stone formation and recurrence.

AUTHOR INFORMATION

Corresponding Authors

Hong-Xing Liu − *Department of Urology, Guangzhou Institute of Urology, Guangdong Key Laboratory of Urology, the First Affiliated Hospital of Guangzhou Medical University, Guangzhou Medical University, Guangzhou, Guangdong 510230, China*; orcid.org/0000-0002-0723-5529; Email: liuhongxing@gzhmu.edu.cn

Xin-Yuan Sun − *Department of Urology, Guangzhou Institute of Urology, Guangdong Key Laboratory of Urology, the First Affiliated Hospital of Guangzhou Medical University, Guangzhou Medical University, Guangzhou, Guangdong 510230, China*; orcid.org/0000-0002-8929-1099; Email: sunxinyuan1985@163.com

Authors

Yi-Han Zhang − *Department of Urology, Guangzhou Institute of Urology, Guangdong Key Laboratory of Urology, the First Affiliated Hospital of Guangzhou Medical University, Guangzhou Medical University, Guangzhou, Guangdong 510230, China*

Chun-Yao Li − *Department of Urology, Guangzhou Institute of Urology, Guangdong Key Laboratory of Urology, the First Affiliated Hospital of Guangzhou Medical University, Guangzhou Medical University, Guangzhou, Guangdong 510230, China*

Guo-Jun Zou − *Department of Chemistry, Institute of Biomineralization and Lithiasis Research, Jinan University, Guangzhou, Guangdong 510632, China*

Jun-Yi Xian − *Department of Urology, Guangzhou Institute of Urology, Guangdong Key Laboratory of Urology, the First Affiliated Hospital of Guangzhou Medical University, Guangzhou Medical University, Guangzhou, Guangdong 510230, China*

Quan Zhang − *Department of Urology, Guangzhou Institute of Urology, Guangdong Key Laboratory of Urology, the First Affiliated Hospital of Guangzhou Medical University, Guangzhou Medical University, Guangzhou, Guangdong 510230, China*

Bang-Xian Yu − *Department of Urology, Guangzhou Institute of Urology, Guangdong Key Laboratory of Urology, the First Affiliated Hospital of Guangzhou Medical University, Guangzhou Medical University, Guangzhou, Guangdong 510230, China*

Ling-Hong Huang − *Department of Urology, Guangzhou Institute of Urology, Guangdong Key Laboratory of Urology, the First Affiliated Hospital of Guangzhou Medical University, Guangzhou Medical University, Guangzhou, Guangdong 510230, China*

Complete contact information is available at: https://pubs.acs.org/10.1021/acsomega.3c01306

Author Contributions

Y.-H.Z., C.-Y.L., and G.-J.Z. contributed equally to this work. Y.-H.Z., C.-Y.L., X.-Y.S., and G.-J.Z. conceived the study and participated in its design and coordination. L.-H.H., B.-X.Y., and H.-X.L. approved the analyzed data and figures; Y.-H.Z., X.-Y.S., and G.-J.Z. wrote and revised the manuscript. All authors have read and agreed to the published version of the manuscript.

Notes

The authors declare no competing financial interest.

ACKNOWLEDGMENTS

This work was granted by the Science and Technology Plan Project of Guangzhou (no: 202102010306) and the Guangdong Provincial Science and Technology Plan Project (no. 2017B030314108).

REFERENCES

(1) Zeng, G.; Mai, Z.; Xia, S.; Wang, Z.; Zhang, K.; Wang, L.; Long, Y.; Ma, J.; Li, Y.; Wan, S. P.; et al. Prevalence of kidney stones in China: an ultrasonography based cross-sectional study. *BJU Int.* **2017**, *120*, 109−116.

(2) Tundo, G.; Vollstedt, A.; Meeks, W.; Pais, V. Beyond Prevalence: Annual Cumulative Incidence of Kidney Stones in the United States. *J. Urol.* **2021**, *205*, 1704−1709.

(3) Dussol, B.; Geider, S.; Lilova, A.; Léonetti, F.; Dupuy, P.; Daudon, M.; Berland, Y.; Dagorn, J. C.; Verdier, J. M. Analysis of the soluble organic matrix of five morphologically different kidney stones. Evidence for a specific role of albumin in the constitution of the stone protein matrix. *Urol. Res.* **1995**, *23*, 45−51.

(4) Ye, Z.; Zeng, G.; Yang, H.; Li, J.; Tang, K.; Wang, G.; Wang, S.; Yu, Y.; Wang, Y.; Zhang, T.; Long, Y.; Li, W.; Wang, C.; Wang, W.; Gao, S.; Shan, Y.; Huang, X.; Bai, Z.; Lin, X.; Cheng, Y.; Wang, Q.; Xu, Z.; Xie, L.; Yuan, J.; Ren, S.; Fan, Y.; Pan, T.; Wang, J.; Li, X.; Chen, X.; Gu, X.; Sun, Z.; Xiao, K.; Jia, J.; Zhang, Q.; Wang, G.; Sun, T.; Li, X.; Xu, C.; Xu, C.; Shi, G.; He, J.; Song, L.; Sun, G.; Wang, D.; Liu, Y.; Wang, C.; Han, Y.; Liang, P.; Wang, Z.; He, W.; Chen, Z.; Xing, J.; Xu, H. The status and characteristics of urinary stone composition in China. *BJU Int.* **2020**, *125*, 801−809.

(5) Schubert, G. Stone analysis. *Urol. Res.* **2006**, *34*, 146−150.

(6) Wesson, J. A.; Ward, M. D. Pathological biomineralization of kidney stones. *Elements* **2007**, *3*, 415−421.

(7) Lieske, J. C.; Swift, H.; Martin, T.; Patterson, B.; Toback, F. G. Renal epithelial cells rapidly bind and internalize calcium oxalate monohydrate crystals. *Proc. Natl. Acad. Sci. U.S.A.* **1994**, *91*, 6987−6991.

(8) Manzanares, D.; Ceña, V. Endocytosis: The Nanoparticle and Submicron Nanocompounds Gateway into the Cell. *Pharmaceutics* **2020**, *12*, 371.

(9) Chaiyarit, S.; Singhto, N.; Thongboonkerd, V. Calcium oxalate monohydrate crystals internalized into renal tubular cells are degraded

and dissolved by endolysosomes. *Chem. Biol. Interact.* **2016**, *246*, 30−35.
(10) Hovda, K. E.; Guo, C.; Austin, R.; McMartin, K. E. Renal toxicity of ethylene glycol results from internalization of calcium oxalate crystals by proximal tubule cells. *Toxicol. Lett.* **2010**, *192*, 365−372.
(11) Wu, J.; Tao, Z.; Deng, Y.; Liu, Q.; Liu, Y.; Guan, X.; Wang, X. Calcifying nanoparticles induce cytotoxicity mediated by ROS-JNK signaling pathways. *Urolithiasis* **2019**, *47*, 125−135.
(12) Zisman, A. L. Effectiveness of treatment modalities on kidney stone recurrence. *Clin. J. Am. Soc. Nephrol.* **2017**, *12*, 1699−1708.
(13) Asadbeigi, M.; Mohammadi, T.; Rafieian-Kopaei, M.; Saki, K.; Bahmani, M.; Delfan, M. Traditional effects of medicinal plants in the treatment of respiratory diseases and disorders: an ethnobotanical study in the Urmia. *Asian Pac. J. Tropical Med.* **2014**, *7*, S364−S368.
(14) Guo, Q.; Chen, Z.; Santhanam, R. K.; Xu, L.; Gao, X.; Ma, Q.; Xue, Z.; Chen, H. Hypoglycemic effects of polysaccharides from corn silk (Maydis stigma) and their beneficial roles via regulating the PI3K/Akt signaling pathway in L6 skeletal muscle myotubes. *Int. J. Biol. Macromol.* **2019**, *121*, 981−988.
(15) Li, Y.; Hu, Z.; Wang, X.; Wu, M.; Zhou, H.; Zhang, Y. Characterization of a polysaccharide with antioxidant and anti-cervical cancer potentials from the corn silk cultivated in Jilin province. *Int. J. Biol. Macromol.* **2020**, *155*, 1105−1113.
(16) Velazquez, D.; Xavier, H.; Batista, J.; de Castro-Chaves, C. Zea mays L. extracts modify glomerular function and potassium urinary excretion in conscious rats. *Phytomedicine* **2005**, *12*, 363−369.
(17) Grases, F.; March, J.; Ramis, M.; Costa-Bauzá, A. The influence of Zea mays on urinary risk factors for kidney stones in rats. *Phytother. Res.* **1993**, *7*, 146−149.
(18) Chen, J. Y.; Sun, X. Y.; Ouyang, J. M. Modulation of Calcium Oxalate Crystal Growth and Protection from Oxidatively Damaged Renal Epithelial Cells of Corn Silk Polysaccharides with Different Molecular Weights. *Oxid. Med. Cell. Longev.* **2020**, *2020*, 6982948.
(19) Zou, G. J.; Huang, W. B.; Sun, X. Y.; Tang, G. H.; Ouyang, J. M. Carboxymethylation of Corn Silk Polysaccharide and Its Inhibition on Adhesion of Nanocalcium Oxalate Crystals to Damaged Renal Epithelial Cells. *ACS Biomater. Sci. Eng.* **2021**, *7*, 3409−3422.
(20) Sun, X. Y.; Ouyang, J. M.; Liu, A. J.; Ding, Y. M.; Gan, Q. Z. Preparation, characterization, and in vitro cytotoxicity of COM and COD crystals with various sizes. *Mater. Sci. Eng., C* **2015**, *57*, 147−156.
(21) Zhao, X.; Ng, S.; Heng, B. C.; Guo, J.; Ma, L.; Tan, T. T.; Ng, K. W.; Loo, S. C. Cytotoxicity of hydroxyapatite nanoparticles is shape and cell dependent. *Arch. Toxicol.* **2013**, *87*, 1037−1052.
(22) Traganos, F.; Darzynkiewicz, Z. Lysosomal proton pump activity: supravital cell staining with acridine orange differentiates leukocyte subpopulations. *Methods Cell Biol.* **1994**, *41*, 185−194.
(23) Paredes, R. M.; Etzler, J. C.; Watts, L. T.; Zheng, W.; Lechleiter, J. D. Chemical calcium indicators. *Methods* **2008**, *46*, 143−151.
(24) Salvioli, S.; Ardizzoni, A.; Franceschi, C.; Cossarizza, A. JC-1, but not DiOC6 (3) or rhodamine 123, is a reliable fluorescent probe to assess $\Delta\Psi$ changes in intact cells: implications for studies on mitochondrial functionality during apoptosis. *FEBS Lett.* **1997**, *411*, 77−82.
(25) Grotto, D.; Maria, L. S.; Valentini, J.; Paniz, C.; Schmitt, G.; Garcia, S. C.; Pomblum, V. J.; Rocha, J. B. T.; Farina, M. Importance of the lipid peroxidation biomarkers and methodological aspects for malondialdehyde quantification. *Quim. Nova* **2009**, *32*, 169−174.
(26) Veeran, S.; Shu, B.; Cui, G.; Fu, S.; Zhong, G. Curcumin induces autophagic cell death in Spodoptera frugiperda cells. *Pestic. Biochem. Physiol.* **2017**, *139*, 79−86.
(27) Chen, S.; Cheng, A.-C.; Wang, M.-S.; Peng, X. Detection of apoptosis induced by new type gosling viral enteritis virus in vitro through fluorescein annexin V-FITC/PI double labeling. *World J. Gastroenterol.* **2008**, *14*, 2174.
(28) Verkoelen, C.; Verhulst, A. Proposed mechanisms in renal tubular crystal retention. *Kidney Int.* **2007**, *72*, 13−18.
(29) Gambaro, G.; Valente, M. L.; Zanetti, E.; Barbera, M. D.; Del Prete, D.; D'Angelo, A.; Trevisan, A. Mild tubular damage induces calcium oxalate crystalluria in a model of subtle hyperoxaluria: evidence that a second hit is necessary for renal lithogenesis. *J. Am. Soc. Nephrol.* **2006**, *17*, 2213−2219.
(30) Schepers, M. S.; Duim, R. A.; Asselman, M.; Romijn, J. C.; Schröder, F. H.; Verkoelen, C. F. Internalization of calcium oxalate crystals by renal tubular cells: a nephron segment-specific process? *Kidney Int.* **2003**, *64*, 493−500.
(31) Liu, Z.; Xiao, Y.; Chen, W.; Wang, Y.; Wang, B.; Wang, G.; Xu, X.; Tang, R. Calcium phosphate nanoparticles primarily induce cell necrosis through lysosomal rupture: the origination of material cytotoxicity. *J. Mater. Chem. B* **2014**, *2*, 3480−3489.
(32) Campos, A. H.; Schor, N. Phyllanthus niruri inhibits calcium oxalate endocytosis by renal tubular cells: its role in urolithiasis. *Nephron* **1999**, *81*, 393−397.
(33) Richards, B. The relation between renal tissue ammonia concentration and ischemic renal damage. *Invest. Urol.* **1971**, *9*, 174−179.
(34) Clapham, D. E. Calcium signaling. *Cell* **2007**, *131*, 1047−1058.
(35) Rizzuto, R.; Pinton, P.; Ferrari, D.; Chami, M.; Szabadkai, G.; Magalhães, P. J.; Virgilio, F. D.; Pozzan, T. Calcium and apoptosis: facts and hypotheses. *Oncogene* **2003**, *22*, 8619−8627.
(36) Hu, S.; Wang, D.; Zhang, J.; Du, M.; Cheng, Y.; Liu, Y.; Zhang, N.; Wang, D.; Wu, Y. Mitochondria Related Pathway Is Essential for Polysaccharides Purified from Sparassis crispa Mediated Neuro-Protection against Glutamate-Induced Toxicity in Differentiated PC12 Cells. *Int. J. Mol. Sci.* **2016**, *17*, 133.
(37) Vakifahmetoglu-Norberg, H.; Ouchida, A. T.; Norberg, E. The role of mitochondria in metabolism and cell death. *Biochem. Biophys. Res. Commun.* **2017**, *482*, 426−431.
(38) Duan, X.; Kong, Z.; Mai, X.; Lan, Y.; Liu, Y.; Yang, Z.; Zhao, Z.; Deng, T.; Zeng, T.; Cai, C.; Li, S.; Zhong, W.; Wu, W.; Zeng, G. Autophagy inhibition attenuates hyperoxaluria-induced renal tubular oxidative injury and calcium oxalate crystal depositions in the rat kidney. *Redox Biol.* **2018**, *16*, 414−425.
(39) Sun, Y.; Liu, Y.; Guan, X.; Kang, J.; Wang, X.; Liu, Q.; Li, D.; Xu, H.; Tao, Z.; Deng, Y. Atorvastatin inhibits renal inflammatory response induced by calcium oxalate crystals via inhibiting the activation of TLR4/NF-κB and NLRP3 inflammasome. *IUBMB Life* **2020**, *72*, 1065−1074.
(40) Wang, J.; Hu, S.; Nie, S.; Yu, Q.; Xie, M. Reviews on Mechanisms of In Vitro Antioxidant Activity of Polysaccharides. *Oxid. Med. Cell. Longev.* **2016**, *2016*, 1−13.
(41) Wang, J.; Guo, H.; Zhang, J.; Wang, X.; Zhao, B.; Yao, J.; Wang, Y. Sulfated modification, characterization and structure−antioxidant relationships of Artemisia sphaerocephala polysaccharides. *Carbohydr. Polym.* **2010**, *81*, 897−905.
(42) Liu, Y.; Tang, Q.; Duan, X.; Tang, T.; Ke, Y.; Zhang, L.; Li, C.; Liu, A.; Su, Z.; Hu, B. Antioxidant and anticoagulant activities of mycelia polysaccharides from Catathelasma ventricosum after sulfated modification. *Ind. Crops Prod.* **2018**, *112*, 53−60.

https://doi.org/10.1021/acsomega.3c01306
ACS Omega 2023, 8, 25839−25849